THE ASTROPHYSICAL JOURNAL, 436:L71–L74, 1994 November 20

NONISOTHERMALITY OF THE HOTTEST CLUSTER ABELL 2163

MAXIM MARKEVITCH[1]
Institute of Space and Astronautical Science, 3-1-1 Yoshinodai, Sagamihara, Kanagawa 229, Japan
I: maxim@astro.isas.ac.jp

AND

KOUJUN YAMASHITA, AKIHIRO FURUZAWA, AND YUZURU TAWARA
Department of Physics, Nagoya University, Furo, Chikusa, Nagoya 461-01, Japan
I: yamasita@satio.phys.nagoya-u.ac.jp,
furuzawa@satio.phys.nagoya-u.ac.jp,
tawara@satio.phys.nagoya-u.ac.jp
Received 1994 June 23; accepted 1994 August 28

ABSTRACT

Preliminary results of the *ASCA* observation of A2163 are presented. Kα lines of He-like and H-like iron have been observed in the SIS spectrum at a redshift of 0.200 (0.190–0.206; hereafter the quoted errors are 90%). The flux ratio in these lines corresponds to $T_e = 16$ keV or a 90% lower limit of 12 keV, unambiguously confirming the presence of very hot gas in this cluster. The GIS spectrum in the 2.5–12 keV band shows a temperature of $T_e = 12.7 \pm 2.0$ keV, and an iron abundance of 0.38 ± 0.13, assuming isothermality. Comparison of the deconvolved GIS cluster images in the energy bands 2.5–7 keV and 7–12 keV (rest frame) shows considerable gas temperature variations in the central 3–4 core radii region. A similar kind of nonisothermality is independently indicated, although marginally, by SIS images in the narrow energy intervals which include the 6.67 keV and 6.97 keV iron line blends. The overall picture suggests that neither the galaxies (Soucail et al. 1994) nor even the gas in A2163 are in equilibrium, and we may be currently observing a merger. If the cluster gas is not isothermal, the somewhat too high temperature derived from the iron line ratio may require a higher iron abundance in the hotter regions of the gas.

Subject headings: galaxies: clustering — X-rays: galaxies

1. INTRODUCTION

A2163, a rich cluster at $z = 0.201$ (Soucail, Arnaud, & Mathez 1994), is one of the hottest and most X-ray–luminous clusters known. Its 2–10 keV luminosity and mean temperature, measured by *Ginga*, are $L_x = 6 \times 10^{45}$ ergs s^{-1} (for $H_0 = 50$ km s^{-1} Mpc^{-1} and $\Omega = 1$) and $T_e = 14$ keV (Arnaud et al. 1992; Elbaz, Arnaud, & Böhringer 1994, hereafter EAB). There is no evidence of a central cooling flow. Combining *Ginga* spectroscopy and *ROSAT* PSPC imaging and assuming isothermality, the latter authors estimated the binding mass of the cluster to be $M(r < 4.6 \text{ Mpc}) = 4.6 \times 10^{15} M_\odot$. A2163 thus represents the extreme high end of the cluster temperature and mass function. The very existence of such clusters has important cosmological implications, e.g., Arnaud et al. (1992); Hattori (1994). A Sunyaev-Zeldovich decrement in the CMBR brightness was detected toward this cluster (Wilbanks et al. 1994), which makes it a candidate for determining the Hubble constant. The above applications require knowledge of the cluster dynamic state and the gas temperature distribution (ideally, in three dimensions), whose estimates have been highly uncertain. Recently Soucail et al. showed that the galaxies in this cluster have a very high velocity dispersion and are not dynamically relaxed. The spectral and imaging capabilities of *ASCA* allow us, for the first time, to map the gas temperature in this cluster on the scale of one to a few core radii. These new measurements indicate that the gas is not isothermal at least in the cluster central part. Below we present some of the preliminary results of the *ASCA* observation of A2163, those which we believe to be less calibration dependent and less affected by the possible systematic errors in this early stage of the *ASCA* data analysis.

2. OBSERVATIONS AND DATA REDUCTION

Instruments onboard *ASCA* (Tanaka, Inoue, & Holt 1994) include two solid-state imaging spectrometers (SISs; Ricker et al. 1994) with an energy resolution of 140 eV at $E = 6$ keV and sensitive in the energy range 0.5–9 keV, and two gas imaging spectrometers (GISs; Makishima et al. 1994), which have a poorer energy resolution but are efficient up to $E = 11$ keV with a larger useful field of view of about 20′ radius. The mirror in front of each detector has a sharply peaked point-spread function (PSF) with about 30″ FWHM and a 3′ half-power diameter (Serlemitsos et al. 1994). Although the temperature of A2163 is too high to be accurately constrained with these instruments, one may be able to perform line diagnostics (e.g., Bahcall & Sarazin 1978) and detect strong spatial temperature variations, if any, on the scale of a few core radii (the cluster core radius is 1′.2; EAB).

A2163 was observed in 1993 August with a useful exposure of 25,000 s, of which 18,500 s is the SIS faint mode data. The cluster gives about 0.5 and 0.4 counts s^{-1} per detector in the 1–12 keV energy band for the GISs and SISs, respectively. We selected the data with a geomagnetic cutoff rigidity >8 GeV c^{-1} to minimize the effects of the background variations and used only the faint mode SIS data, most suitable for accurate spectroscopy. The SIS results presented here are insensitive to the background subtraction. To subtract the GIS background, we used a massif of the blank sky observations with a total

[1] Permanent address: Space Research Institute (IKI), Profsoyuznaya 84/32, Moscow 117810, Russia. I: maxim@hea.iki.rssi.ru.

exposure over 300 ks, normalizing it individually for each cutoff rigidity interval according to the exposures.

3. SPECTRA

Cluster spectra from the two GISs in the energy band 2.5–12 keV, collected from an 8′ radius circle centered on the brightness peak, are consistently fitted separately and well fitted simultaneously ($\chi^2 = 23.5/38 - 3$ d.o.f.) by an isothermal plasma emission model (Raymond & Smith 1977, 1992 revision) with $T_e = 12.7 \pm 2.0$ keV and an iron abundance relative to solar (Allen 1973) of 0.38 ± 0.13 (single-parameter intervals, fixing $z = 0.2$; the quoted errors are 90% throughout the *Letter*), reasonably insensitive to the hydrogen absorption column, fixed at EAB's 1.65×10^{21} cm^{-2}. We excluded the energy band below 2.5 keV because the calibration of the instrument at those energies is still uncertain at the time of this writing. To get the mirror spectral response in the interesting detector region, a symmetric brightness model with $a_x = 1'.2$ and $\beta = 0.62$ (EAB), multiplied by the mirror effective area and convolved with its PSF has been used. The obtained temperature is marginally consistent, and the abundance is in a good agreement with the *Ginga* values, 14.6 ± 0.9 keV and 0.40 ± 0.15 (EAB). For a 5′ radius integration region, the best-fit temperature is the same and the abundance is within the statistical error. An accurate measurement of the temperature differences on a large linear scale, including an average temperature change with the cluster radius, will be presented in a later paper. A less calibration-dependent attempt to detect temperature changes on a small scale of one to a few core radii is presented in § 4.

In the SIS spectra, the two lines have been detected at 5.55 keV and 5.80 keV (Fig. 1), obviously identified as He- and H-like iron Kα lines at $z = 0.200$ (0.190–0.206). To measure the line positions, we co-added spectra from the two detectors, fitted and subtracted the continuum in the interval 3.5–7 keV excluding the lines,[2] and cross-correlated the residual with the model lines, for which Mewe, Gronenschild, & van den Oord (1985) data convolved with the detector response have been used. The resulting redshift value is independent of the temperature assumed in the line model and of the continuum fit. A possible systematic error from the SIS gain miscalibrations is likely to be a small fraction of the statistical error (R. Fujimoto, private communication).

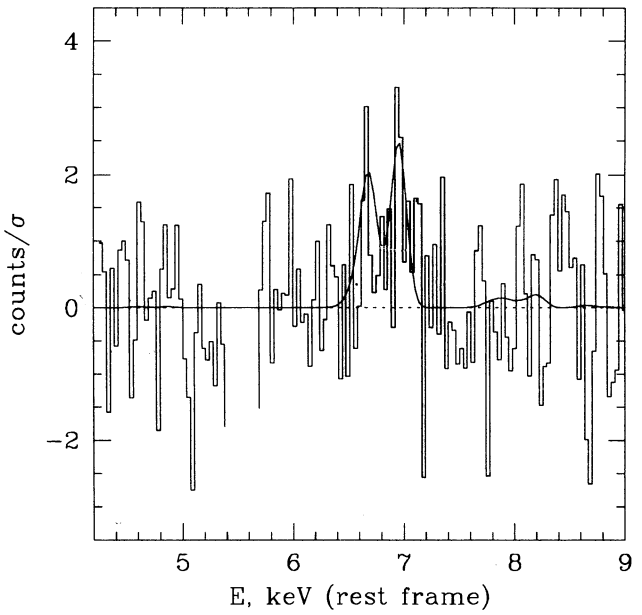

FIG. 1.—Part of the combined SIS cluster spectrum featuring He- and H-like iron Kα lines, with the local continuum subtracted. To get the redshift, Mewe et al. line data for $T_e = 15$ keV have been convolved with the detector response to model the lines (smooth line) and then cross-correlated with the residual. A flux for each line has been calculated by convolving the residual with a detector response to the δ-function at that line's energy, taking into account the small uncertainty of the continuum estimate.

The ratio of the fluxes in these lines is a useful indicator of the gas temperature, independent of an overall spectrum model and unlikely to be affected by any miscalibration. In the spectrum of the whole cluster (collected from the two chips which essentially include the central 5 core radii region), the absolute fluxes in these lines are $(2.3 \pm 1.3) \times 10^{-5}$ and $(3.6 \pm 1.3) \times 10^{-5}$ counts cm^{-2} s^{-1}, and the line equivalent widths are 80 ± 46 eV and 133 ± 50 eV, respectively (the equivalent width values are tentative since they are background-dependent). Assuming collisional ionization equilibrium and isothermality, the line flux ratio corresponds to $T_e = 16$ keV, or a 90% lower limit of 12 keV (R. Mewe 1994, private communication; 17 keV and >13 keV, respectively, using either the Mewe et al. 1985 or Raymond & Smith data). This is somewhat higher but at this accuracy consistent with the GIS estimate from the continuum. The total equivalent width of these two lines corresponds to an iron abundance of 0.38 ± 0.12, taking for example, the GIS best-fit temperature of 13 keV; the higher the assumed temperature the higher the abundance.

4. SPECTRO-IMAGING

The appearance of the GIS and SIS images in the softer and harder energy bands suggests the existence of hardness ratio variations in the central part of the cluster. However, the mirror PSF strongly depends on energy and position in the focal plane, which distorts softer and harder images differently, something especially serious for a cluster like A2163 with an angular size comparable to that of the PSF. To take this effect into account, we attempted to deconvolve the GIS images in the energy intervals 2–6 keV and 6–10 keV (receiver frame), excluding the softer band with a wider detector PSF and not unlikely spatial variations of the absorption column density (known to be excessive toward this cluster; Arnaud et al. 1992). For simplicity of the algorithm (described in Appendix), we used data only from the GIS whose field of view comprises the whole cluster. The resulting images, representing the sky brightness, are shown in Figure 2. The soft-band image resembles the *ROSAT* PSPC (EAB) and the earlier *Einstein* IPC (Ulmer, Kowalski, & Cruddace 1986) images. Comparison of the deconvolved images reveals at least two regions of the cluster with a hardness ratio significantly different from that in the center. In the eastern and northwestern regions shaded in Figure 2*b*, the hardness ratio corresponds to the temperatures below 7 keV and above 13 keV at a formal 90% confidence, respectively. To ensure that imperfection of the ray-traced mirror PSF which we used is not responsible for the detected effect, we also used as a PSF the GIS images of Cyg X-1, observed at a focal plane position close to that of the cluster

[2] Parameters of the bremsstrahlung continuum fit are background dependent and not meaningful at this stage of the analysis. This uncertainty does not affect either the measured line positions or their fluxes.

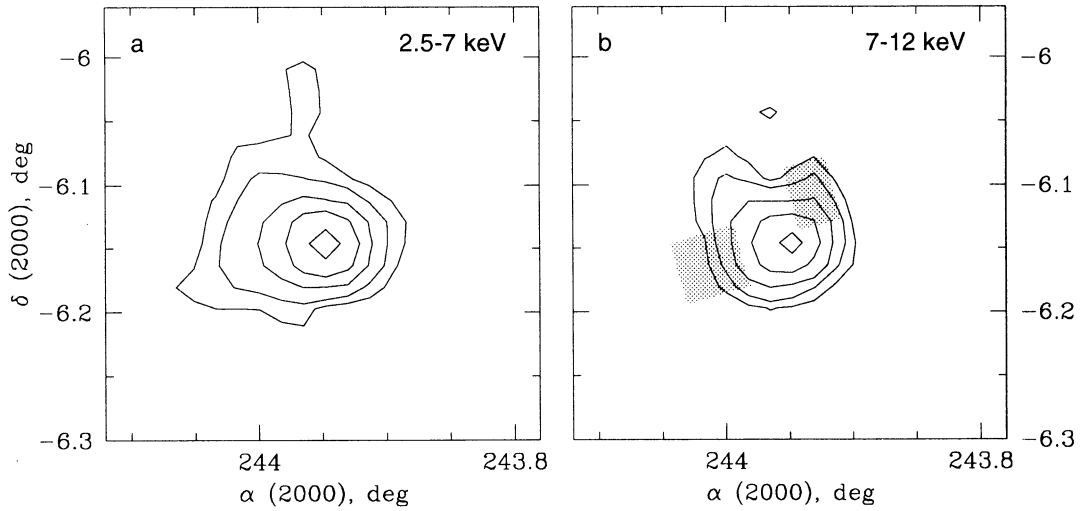

FIG. 2.—Deconvolved GIS images of the cluster, reconstructed on a 1′ grid. Energy bands are given in the cluster frame (2–6 and 6–10 keV receiver frame), contours are in arbitrary units of the sky brightness and spaced by a factor of 2. Shaded are two regions with hardness ratios significantly different from that in the center. In the eastern and northwestern regions, $T < 7$ keV and $T > 13$ keV at the 90% confidence, respectively. The input GIS images have in total about 16,000 and 1800 photons from the cluster in the softer and harder energy band, respectively.

center, and obtained qualitatively the same picture. The GIS background brightness is less than 10% of the cluster brightness in these regions in both energy bands, and its uncertainties cannot produce such a difference. The harder region to the northwest is also seen in the SIS images in the same energy bands (while the softer spot is outside its field of view), although we did not perform deconvolution of the SIS images. Thus the hardness ratio variations are unlikely to be an artifact, although for a more quantitative estimate there is not enough statistics and confidence in the instrument calibration.

Given this evidence of the temperature variations from the hardness ratio map, it is interesting to see if there is a similar difference in the spatial distribution of the emission in the He- and H-like iron lines observed in the SIS spectrum, even though their statistics is very poor (there are only about 50 and 75 photons from each line, respectively). Figure 3 shows images (a sum of the two SISs) in the 0.25 keV energy intervals centered at each line, with the continuum emission crudely subtracted, for which an image in the adjacent energy interval 4–5.4 keV has been taken and normalized according to each line's equivalent width. Because the lines have close energies, these images can be compared directly. We performed a simple χ^2 test of the 1′-binned images (without the continuum subtraction), in which the images without the continuum subtraction were normalized to have the same number of photons, and then $\chi^2 = \Sigma(x_1 - x_2)^2/(\sigma_1^2 + \sigma_2^2)$ was calculated over the 1′ pixels, x_1 and x_2 denoting the pixel values in the two images and σ_1 and σ_2 denoting their errors. The test shows that central 4′ × 4′ parts of the two images are different at the 97% confidence level ($\chi^2 = 27/15$ d.o.f.), while images in the adjacent

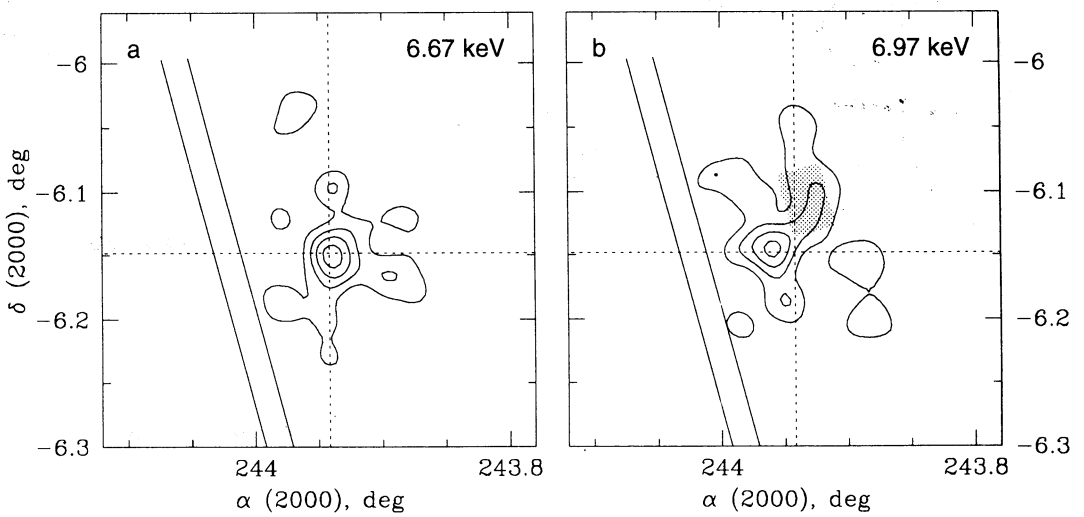

FIG. 3.—Co-added smoothed SIS images in the 0.25 keV bands including the He- and H-like iron lines at 5.55 keV and 5.80 keV (receiver frame), with the continuum image crudely subtracted. Contours are in arbitrary units of the detector brightness and linearly spaced. The images have in total only about 50 and 75 photons. Central 4′ × 4′ parts of the images are different at the 97% confidence. In the brightness peaks of the He- and H-like lines, the line flux ratio corresponds to $T_e \simeq 7$ keV and 24 keV, respectively. Shaded is the hotter region from Fig. 2; there is likely to be an H-like line emission excess as well, supporting a higher gas temperature in that region. Parallel lines are boundaries of the two SIS.

energy intervals of the same width, not containing the lines, were consistent, with $\chi^2 = 9/15$ d.o.f. To get an idea of the physical scale of the differences, in the cluster center where the He-like line emission is apparently peaked, and in the H-like line brightness peak displaced by 1′–2′, the line flux ratio corresponds to $T_e \simeq 7$ keV and 24 keV, respectively. These peaks appear too close to be resolved in the GIS data with the deconvolution algorithm we used. Shaded in Figure 3*b* is the hotter region from the GIS deconvolved images. The figure shows a likely excess of the H-like iron line intensity in that region as well, suggesting that the higher hardness ratio is indeed due to hotter gas rather than something nonthermal.

5. DISCUSSION

Although the results from the GIS image deconvolution are only qualitative for now and the SIS iron line images alone are not persuasive because of the poor statistics, both methods independently and consistently suggest considerable spatial temperature variations in the central few core radii region of the cluster. It is interesting to note that optical spectroscopic data on 80 galaxies within a 6.′5 × 6.′5 central region of this cluster (Soucail et al.) show a very high velocity dispersion and significant subgrouping in the coordinate-redshift galaxy distribution, indicating that the galaxies are in a highly nonrelaxed state. One of the possible subgroups apparently coincides with our hotter region in the northwest. It is unlikely, however, that we are observing an infalling group that retained its atmosphere, as may be the case, for example, in A2256 or Coma (Briel, Henry, & Böhringer 1992; White, Briel, & Henry 1993), since to contain a hotter gas, the group would have to be dense and appear in the softer images as a gas density enhancement. The hotter spots we observed near the cluster center and to the northwest and the cooler spot to the east may instead be nonstatic regions of gas produced in the process of a merger, like those in, e.g., the simulations of Schindler & Müller (1993). The overall picture, including the optical data and the cluster high temperature, may suggest an ongoing merger, perhaps proceeding in the *z*-direction. From the morphology of their image at lower energies, EAB also suggested a possible recent merger. Analysis of the large-scale temperature structure of A2163 is underway, which should tell whether there are other features in the temperature distribution characteristic to a merger. With not much better statistics, high-velocity gas flows like those in merger simulations by Schindler & Müller and Roettinger, Burns, & Loken (1993) may also be detectable by spatially resolved measurement of the redshift of the iron lines.

If the gas is considerably nonisothermal, it may be difficult to reconcile a somewhat higher temperature estimate derived from the SIS iron lines ratio with the lower estimates from the continuum fit, since for a mixture of gas with different temperatures from the interesting range of 7–20 keV, a line ratio estimate should instead be lower. One could then satisfy the continuum temperature estimate, the line ratio and their equivalent widths by assuming, for example, a higher abundance in the hotter regions of the gas, motivating it by a more active removal of iron off the galaxies in the regions of shocks and gas flows, the places where the gas is being heated during the merger. There are too few photons from the iron lines for a direct measurement of the abundance in different regions of A2163, but, e.g., in the Perseus cluster, Arnaud et al. (1994) have indeed noticed a hotter region of the gas with a higher iron abundance.

It is a pleasure to acknowledge the successful work of the many people involved in the launch, operation, and calibration of *ASCA* and in creating the data processing software. We thank G. Soucail and collaborators for giving us their data prior to publication, and R. Mushotzky, A. Antunes, and the referee for useful comments on the manuscript. M. M. would like to thank JSPS and ISAS for their support and hospitality during this work.

APPENDIX

IMAGE DECONVOLUTION

We call "image deconvolution" the least-squares solution of the linear system $P_i E_i x = y_i$ $(i = 1, 2)$, $\Delta x = 0$, where x is the model image, to which E_i, multiplication by the mirror effective area, and P_i, redistribution of photons by the mirror PSF (both dependent on energy and position), are applied, and y_i is an image from the ith GIS. A regularizing condition $\Delta x = 0$, taken with a small relative weight, enforces smoothness of the solution. (The mirror optical axes are at different positions so E and P are different for the two GIS, and the system is overdetermined even without regularization, making the problem better posed than an image deconvolution in its usual meaning, as that, e.g., in Press et al. 1992.) The solution (brightness in each pixel of x) was found iteratively, taking as a zero approximation the symmetric β-model. The GIS images were smoothed to compensate for different detector PSF at different energies and binned to 25 × 25 1′ pixels. The errors have been conservatively overestimated by Monte Carlo simulations, adding random noise to the data and rerunning iterations.

REFERENCES

Allen, C. W. 1973, Astrophysical Quantities (London: Athlone)
Arnaud, M., Hughes, J. P., Forman, W., Jones, C., Lachieze-Rey, M., Yamashita, K., & Hatsukade, I. 1992, ApJ, 390, 345
Arnaud, K. A., et al. 1994, ApJ, 436, L67
Bahcall, J. N., & Sarazin, C. L. 1978, ApJ, 219, 781
Briel, U. G., Henry, J. P., & Böhringer, H. 1992, A&A, 259, L31
Elbaz, D., Arnaud, M., & Böhringer, H. 1994, A&A, submitted (EAB)
Hattori, M. 1994, ApJ, 426, 19
Makishima, K., et al. 1994, in preparation
Mewe, R., Gronenschild, E. H. B. M., & van den Ord, G. H. J. 1985, A&AS, 62, 197
Press, W. H., Teukolsky, S. A., Vetterling, W. T., & Flannery, B. P. 1992, Numerical Recipes (Cambridge: Cambridge Univ. Press)
Raymond, J. C., & Smith, B. W. 1977, ApJS, 35, 419
Ricker, G., et al. 1994, in preparation
Roettinger, K., Burns, J., & Loken, C. 1993, ApJ, 407, L53
Schindler, S., & Müller, E. 1993, A&A, 272, 137
Serlemitsos, P., et al. 1994, in preparation
Soucail, G., Arnaud, M., & Mathez, G. 1994, in preparation
Tanaka, Y., Inoue, H., & Holt, S. S. 1994, PASJ, 46, L37
Ulmer, M. P., Kowalski, M. P., & Cruddace, R. G. 1986, ApJ, 303, 162
White, S. D., Briel, U. G., & Henry, J. P. 1993, MNRAS, 261, L8
Wilbanks, T. M., Ade, P. A. R., Fischer, M. L., Ho, T. R., Holzapfel, W. L., Osgood, D. E., & Lange, A. E. 1994, ApJ, 427, L72